Proceedings of the Canadian Society for Mechanical Engineering International Congress 2022

CSME Congress 2022

June 5-8, 2022, Edmonton, AB, Canada

The effects of the reservoir geometry on the velocity distribution in a simple microchannel

Zahra Maleksabet[1*], Azam Zare[2], Ali Tarokh[1]

[1] Department of Mechanical Engineering, Lakehead University, Thunder Bay, Ontario, P7B5E1, Canada

[2]BioMEMS and Bioinspired Microfluidic Laboratory, Department of Mechanical and Manufacturing Engineering, University of Calgary, Calgary, Alberta T2N 1N4, Canada.

[*]zahramaleksabet76@gmail.com

Abstract— Capillary microfluidics is gaining popularity due to its role in recent advances in life science applications. Designing a new and optimized microfluidic platform, as well as having a broader understanding of its function and fundamental physics, are still significant technological problems. However, numerical simulations reveal underlying mechanisms and examine various geometrical effects in microfluidics. In this study, the influence of reservoir geometry in the shape of a circle, square, and rectangle on capillary flow in the microchannel was explored numerically. This study was done by running two-phase flow level set model simulations using the Finite Element Method. The capillary flow characteristics in a microfluidic design were investigated, as well as the filling time, velocity, and pressure drop for various reservoir geometries. The computational result was validated against the analytical solution. It has been demonstrated that the reservoir geometry changes liquid velocity in a microchannel. Microchannel filling time is shorter for the circular reservoir geometry. Therefore, reservoir geometry can be considered a parameter in designing and optimizing a microfluidic platform.

Keywords-component; Reservoir geometry; Interface position; Microfluidics; Capillary flow; Two-phase flow

I. INTRODUCTION

Microfluidics exhibits unique phenomena that can be leveraged to fabricate devices and components capable of performing functions useful for many biological studies [1-7]. The bioanalytical devices capable of analyzing complex biological samples have application in several diverse areas such as clinical diagnostics, drug discovery, and biohazard detection. For instance, in the recent COVID-19 pandemic, microfluidics played a significant role in controlling the spread of the pandemic and choosing a suitable treatment plan, a fast, accurate, effective, and ready-to-use diagnostic method [8-11]. Many functional components for microfluidic devices have been developed to make them more applicable, such as micropump, micromixer, reservoir, retention valve, and trigger valve. However, some of these devices, like micropumps, require electrical control and power suppliers [12]. Capillary action is a liquid driving force, and liquid penetrates the capillary channel by capillary action at the gas-liquid interface. Capillary action eliminates the need for micropumps and electrical power. Also, any optimization in the geometry of the components of the microfluidics device can reduce the cost of microfluidics applications [12-19].

Ichikawa et al. [12] examined the motion of the interface in a microchannel with a rectangular cross-section using capillary force, and the experimental results were compared with the theoretical one. They obtained the value of a dimensionless driving force related to dynamic contact angles. Using this variable, interface motion can be predicted for any size of rectangular channels. Taher et al. [18] studied a microchannel facing a backward-facing step (BFS). In the theoretical study, a 2D interface model was assumed, and the capillary pressure was known as a function of the length of the microchannel and the contact angle. The simulation study, which was done in two ways of minimizing the interface energy method and volume of fluid method, showed good agreement with the theoretical study. Comparing three different contact angles and three different aspect ratios for the microchannel indicated that the more the contact angle and aspect ratio, the more agreement with the experimental study is. The experimental model was presented in 5 aspect ratios, and they showed good agreement with the theoretical study. Ma [14] assessed the capillary performances of wicking structures consisting of parallel microchannels analytically and numerically. The capillary rate-of-rise curve for water was compared between parallel microchannel configurations with different dimensions and cross-sectional shapes. The results demonstrated that adopting a noncircular cross-sectional shape can improve the capillary flow rate by up to 32% due to the lower friction factor but the same level of capillary force. Mikaelian et al. [15] investigated a modeling framework for capillary-driven flow in closed complex microfluidic networks using electric circuit analogy. The model handles two immiscible fluid phases, including the capillary pressure jump across the interface between the phases, in a large variety of fluidic structures. Splitters, mixers, micropillar arrays, tapered or open channels can be modeled and combined to form unique complex networks. As outputs, the position and velocity of each interface in the analyzed microfluidic network were provided as a function of time. Guo

et al. [13] investigated the pressure drop of a tree-typed microchannel, numerically and experimentally. CO2 and AMP were two phases of the flow, respectively. The pressure difference consists of the pressure drop across a liquid slug, the pressure drops across the body of a bubble, and the interfacial pressure drop over two caps of a bubble. The body shortening stage and cap shrinking stage in the microchannel cause some differences in pressure drop. The experimental pressure drop was almost the same as the theoretical one in a single microchannel by a 5% difference by not considering the mass transfer.

Although mainly the dimensions of the microchannel and its changes in fluid flow were considered, the changes in the geometry of components for a microfluidic device were rarely studied. Reservoir is one of the primary components that its changes can significantly impact the fluid flow.

However, the experiments are the most reliable way of investigating in the field of microfluidics; it faces lots of difficulties. Due to the nano and micro dimensions, sensors are limited and cannot measure every parameter of the fluids [15]. Also, the experiments can take a long time and be expensive for a diverse range of fluids and geometries. On the other hand, theoretical studies consist of many assumptions and simplifications that make the model far from reality. Simulations and numerical studies are the best methods for investigating microfluidics for different fluids and geometries. Numerical study of microfluidics can be done at a much lower cost than experimental studies with acceptable accuracy using different numerical methods.

II. METHODOLOGY

One of the primary elements of the microfluidic circuits is the reservoir, which is used as a container and releases the precise, predetermined volume of liquid. Reservoirs are presented in different sizes and geometries depending on the microfluidics circuits [16]. In this article, the effects of the reservoir geometry on a capillary flow in a simple microchannel are numerically studied using the Multiphysics module of COMSOL software. A two-phase flow consisting of air (the gas) and water (the liquid) is modelled, and the position and velocity of the interface and the pressure distribution are plotted and discussed. Also, the simulation result is validated by the analytical solution of the capillary flow in a simple microchannel.

A. Governing Equations

The fluid flow in a simple channel is considered as a laminar incompressible two-phase flow of two immiscible fluids of water and air. The dynamic of fluid flow is described by the unsteady incompressible Navier–Stokes equations. The continuity and momentum equations are presented in Equations (1) and (2) [10].

$$\nabla . \boldsymbol{u} = 0 \tag{1}$$

$$\rho\, \partial \boldsymbol{u}/\partial t + \rho(\boldsymbol{u}.\nabla)\boldsymbol{u} = \nabla.[-p\boldsymbol{I} + \mu\,(\nabla \boldsymbol{u} + (\nabla \boldsymbol{u})^T)] + \rho \boldsymbol{g} + \boldsymbol{F\_st} \tag{2}$$

where u (m/s), ρ (kg/m^3), μ (Pa.s), p (Pa) and g (m/s^2) are flow velocity vector, density, dynamic viscosity for the water or the air, flow pressure, and gravity vector, respectively. The identity matrix is denoted by the letter "I". Besides, for two-phase flow, F_st is the surface tension force acting at the air-water interface. The surface tension force is defined as Equation (3), calculated at the Level Set interface [10].

$$\boldsymbol{F\_st} = \nabla . \boldsymbol{T} \tag{3}$$

$$\boldsymbol{T} = \sigma\,(\boldsymbol{I} - (\boldsymbol{nn}\text{^}T))\delta \tag{4}$$

$$\boldsymbol{n} = \nabla\phi/|\nabla\phi| \tag{5}$$

σ (N/m) is the surface tension coefficient, and δ is a nonzero Dirac delta function at the two-phase fluid interface. The interface normal vector n is in terms of the level set function. The level set interface function is a smooth continuous function that is denoted by $0 \le \phi \le 1$. The level set function of 0.5 represents the fluid interface, and ϕ equals 0 and 1 for the air and the water, respectively. The fluid interface between the two phases is given by Equation (6) for the level set method [10].

$$\partial\phi/\partial t + \boldsymbol{u}.\nabla\phi = \gamma\nabla.(\varepsilon\nabla\phi - \phi(1-\phi)\ \nabla\phi/|\nabla\phi|) \tag{6}$$

The numerical stabilization parameters are ε and γ, where ε is interface thickness, and γ is the reinitialization parameter which is equal to the maximum velocity magnitude occurring in the model. The liquid column length or liquid/air interface position for capillary flow in a microchannel is determined by integrating the level set function along the length of the microchannel at each time step. The viscosity and density of the fluids at the interface are specified by Equations (7) and (8), respectively[10].

$$\rho = \rho\_air + (\rho\_water - \rho\_air)\phi \tag{7}$$

$$\mu = \mu\_air + (\mu\_water - \mu\_air)\phi \tag{8}$$

B. Theoretical Approach

Under low-Reynolds-number conditions, fluid dynamics in microfluidics are laminar. In microscale, surface tension forces at liquid/air interfaces are much stronger, with the capillary force acting as the driving force. The capillary pressure jump across an interface for a closed rectangular microchannel is presented by Equation (9) [15]:

$$\Delta p = \sigma\left(\frac{\cos\theta_{left} + \cos\theta_{right}}{W} + \frac{\cos\theta_{top} + \cos\theta_{bottom}}{H}\right) \tag{9}$$

Where W and H are the channel's width and height, respectively, and θ is the contact angle of the liquid with different walls of the microchannel.

Ichikawa et al. [12] found an exact solution for the laminar flow velocity distribution in a cross-section of a rectangular channel with no-slip boundary conditions at the channel walls.

$$u = \left(\frac{8H^2}{\pi^4\mu}\right)\sum_{n=0}^{\infty}\frac{1}{(2n+1)^4}\left\{1-\frac{1}{X(n)}\tanh X(n)\right\} \quad (10)$$
$$X(n) = \frac{(2n+1)\pi W}{2H}$$

Therefore, if we use the first term of the summation ($n = 0$), after integrating Equation (10), the liquid column length or the liquid/air interface position (IP) is simplified as follows in Equation (11):

$$IP_{Analytic} = sqrt\left(\frac{16H^2}{\pi^4\mu}\left\{1-\frac{2H}{\pi W}\frac{\pi W}{2H}\right\}\Delta p\right)\sqrt{t} \quad (11)$$

t is the microchannel filling time.

C. Simulation Study and Computational Domain

The microchannel design has a width of $300\mu m$, a height of $80\mu m$, and a length of $2cm$. The properties of the two fluids are considered at a temperature of 300K.

The capillary pressure pushes the flow through a microchannel, and its magnitude depends on the surface tension of the liquid in two-phase flow and the contact angle of the fluid with the channel walls. A surface is considered wettable if the surface contact angle of the liquid on that surface is <90°. Microchannels with wettable surfaces generate a concave liquid-air interface and a negative capillary pressure that spontaneously wicks liquid into the conduit by capillary force. The interface is convex for surface contact angles >90°, and the positive pressure pushes the liquid out of the channel [16]. In this study, the static contact angle with water is considered as 40.03° for top and bottom walls to create wettable walls and negative capillary pressure. For left and right walls, the value of static contact angle is considered as 96.81°, so the capillary pressure is positive.

The microchannel design is simulated with a 3D model in the Multiphysics Module of COMSOL software using the Finite Element method by solving Equations (1) to (8). The pressure at the inlet and outlet boundary conditions is assumed to be atmospheric pressure. An extended microchannel and three different geometries for reservoirs with the same volume of 0.5 μl for reservoir are proposed (Figure 1i)), and the microchannel with every reservoir is simulated to investigate the differences in the velocity and position of the interface and pressure distribution for each reservoir:
(1) square shape: side = $2.5mm$
(2) rectangular shape: length = $3.125mm$ and width = $2mm$
(3) circular shape: diameter = $2.82mm$

The 3D computational domain was meshed by the extra fine hexahedral elements, and the dependence of the interface position and velocity on the number of mesh elements was evaluated through a grid convergence study (Figure 1ii)).

III. Result and Discussion

D. Validation of the Simulation

In this section, the numerical simulations are validated with the results from the analytical solution (Equation (11)). The analytical solution and the numerical results for (a) the position and (b) the velocity of the water-air interface are shown in Figure 2. The velocity and interface position is in good agreement with the analytical solution. The velocity of the interface is estimated high at the beginning of the channel from both numerical and analytical results. However, as the flow resistance increases, the velocity decreases with respect to time. It indicates the significance of precisely modeling the velocity at the channel entrance. In Figure 2b), as the flow passes the

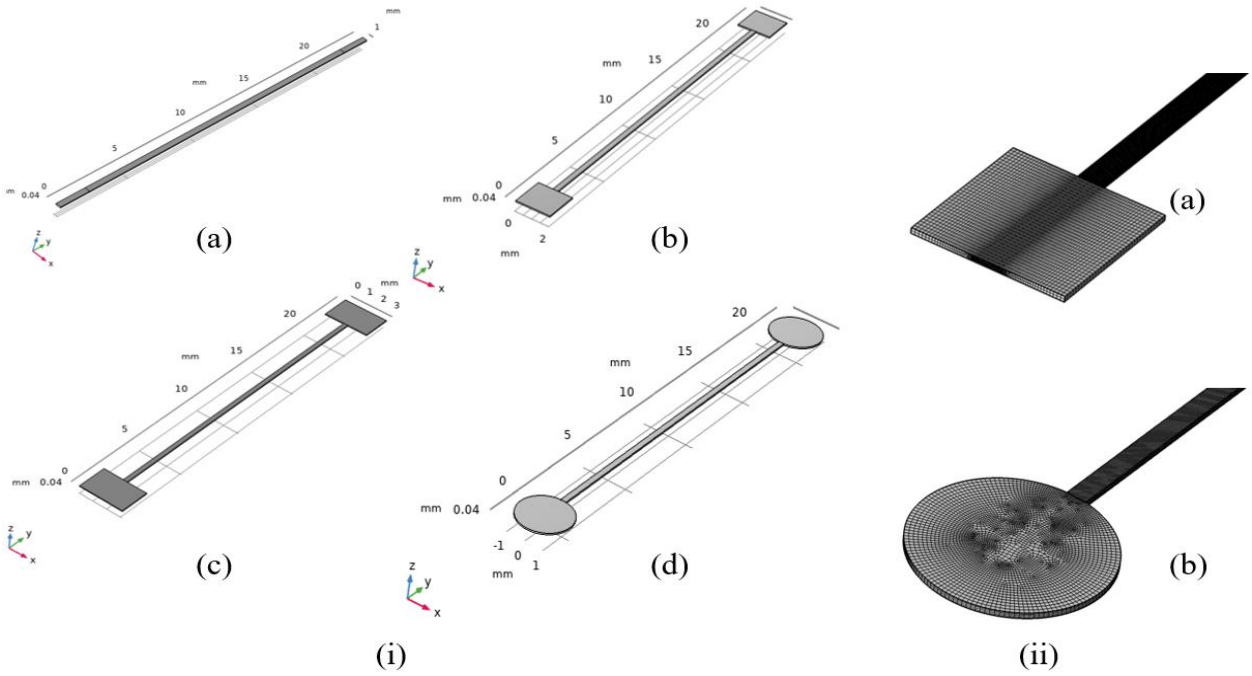

Figure 1: (i) Microchannel with different reservoirs (a) extended channel, (b) square reservoir, (c) rectangular reservoir, (d) circular reservoir, (ii): (a) square reservoir, (b) circular reservoir

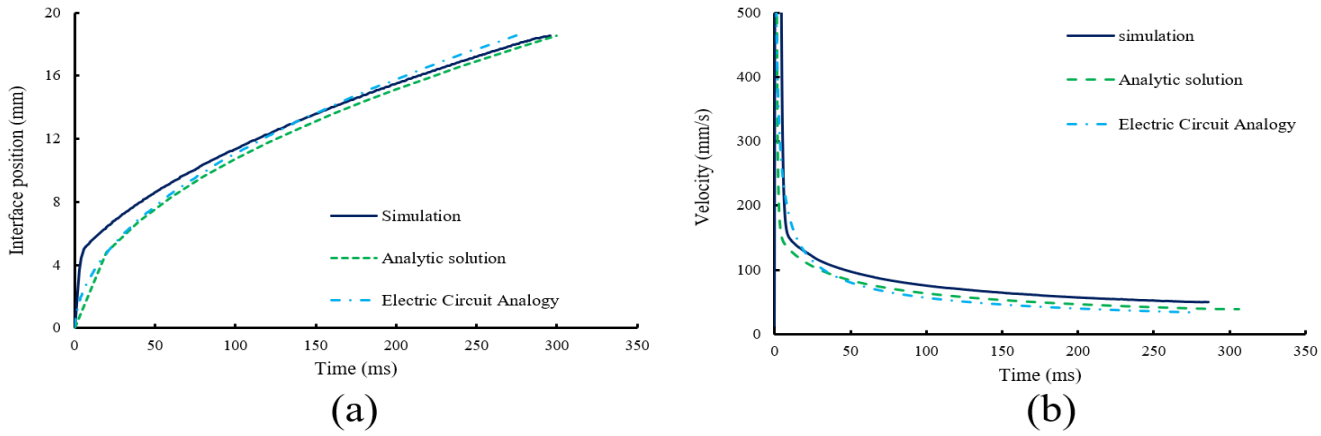

Figure 2: (a) interface position across the length of the channel over time, (b) velocity of the interface over time.

transient mode, velocity changes become less, and the velocity turns to a constant value and as a result, in Figure 2a), by spending the time, the plot becomes linear.

Moreover, simplified numerical modeling in electric circuit analogy for Ohm's law has been used to prescribe the flow/pressure relation in microfluidic platforms. According to the well-known hydraulic–electric circuit analogy, the volumetric flow rate (Q) through a microchannel is proportional to the capillary pressure (ΔP) and inversely proportional to its hydraulic resistance R ($\Delta P = RQ$) [15]. The capillary pressure difference at the interface of the liquid in a rectangular channel can be described by Young–Laplace Equation (9) [12]. The Ohm's law equation can be solved for a given position of the liquid-gas interface to find the Q and fluid flow velocity. Figure 2a) and (2b) compare the simulation results and the data generated by the numerical solution of the capillary flow in the microchannel in analogy to the electric circuit for the position and velocity of the liquid interface.

E. Effects of the reservoir shape on the flow

Three different shapes are selected for the reservoir, and their geometry effects on the position and velocity of the interface in the channel are investigated.

In Figure 3, the extended microchannel and three reservoir geometries (circular, square, and rectangular) are compared in terms of (a) the interface position and (b) velocity over time. Results show that the liquid moves faster when the circular reservoir is utilized. This happens due to the less pressure loss caused by the corners at the intersection of the reservoir and the channel. Therefore, for the circular design, capillary pressure overcomes the flow resistance at the entrance of the microchannel, and the liquid moves through the microchannel faster. Moreover, computational results show that flow velocity for the rectangular design is less than the square design.

Figure 4 confirms the results in Figure 3 with the help of velocity contour for each reservoir design. As shown in Figure **4**, a circular reservoir guides the fluid flow to the microchannel, while square and rectangular reservoirs slow the fluid flow in the entry of the channel.

F. Velocity Distribution

Figure **5**i) shows the level set contour at the time when the liquid reaches the mid-length of the channel (L=10mm). It is considered that the flow reached the middle of the channel at a specific time for each microfluidic design, and this time is increasing from the extended channel to circular, square, and rectangular reservoir. At the same time, Figure **5**ii) and Figure **5**iii)

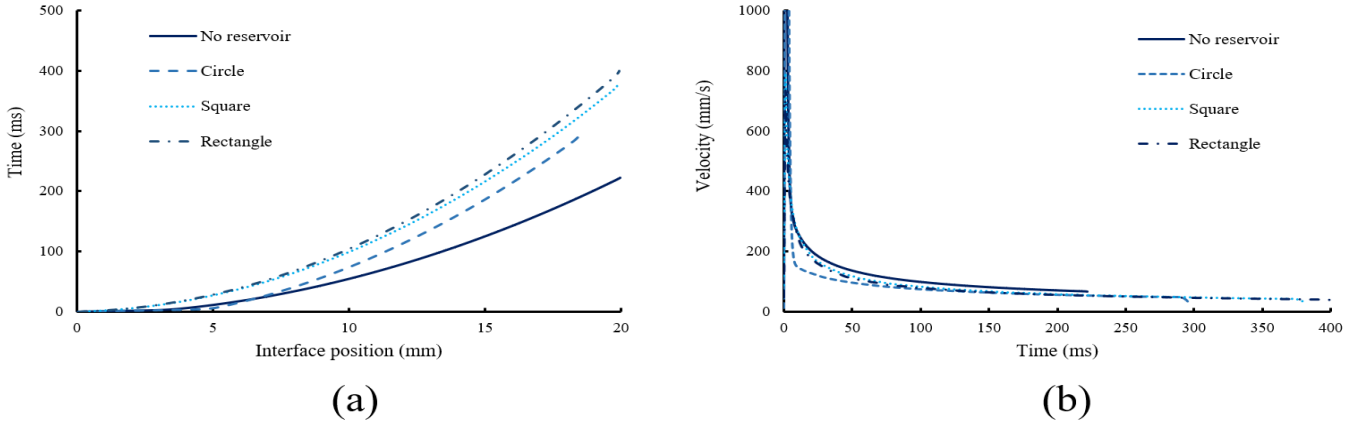

Figure 3: (a) interface position across the length of the channel over time for different reservoirs, (b) velocity of the interface over time for different reservoirs.

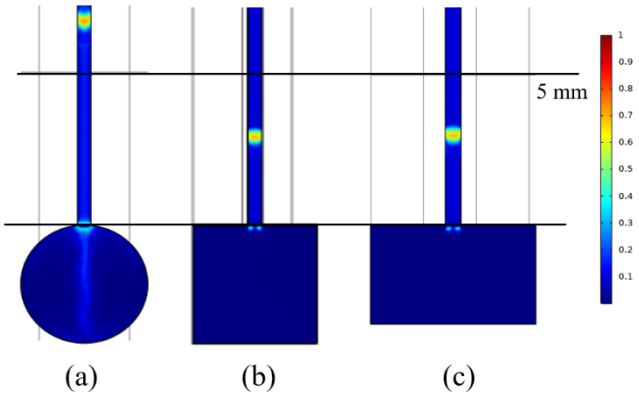

Figure 4: velocity contour for (a) circular reservoir, (b) square reservoir, (c) rectangular reservoir.

show velocity distribution in microchannel cross-sections along the width and height of the channel in the x and z directions, respectively. As it was mentioned in section C, the top and bottom walls are hydrophilic and the left and right walls are hydrophobic so by considering the velocity profile at the interface position of L=10*mm*, it is shown that first, the velocity has the concave shape respect to the properties of walls and second, the velocity is high near the walls which can prove that the capillary force pushes the liquid through the channel, and then it becomes less in the middle of the cross-section.

Moreover, the velocity distribution at two other times before and after the time that liquid reaches the L=10*mm* for water and air, respectively are shown in Figure 5ii) and (5iii). As it is expected for the laminar flow in a channel and no-slip boundary condition, the velocity profile of the water and air at a cross-section of the microchannel is parabolic in shape with the maximum velocity at the center.

G. pressure distribution across the channel

Pressure distribution for the extended microchannel and three reservoir shapes is shown in Figure 6. Due to the initial boundary condition, inlet gauge pressure is zero across the microchannel, and it becomes less till it faces the interface at three different times. At the interface, a pressure jump occurs because of the capillary pressure. Therefore, the point of discontinuity of the pressure along the microchannel length indicates the interface position. Moreover, the value of the pressure difference along the length of the microchannel for

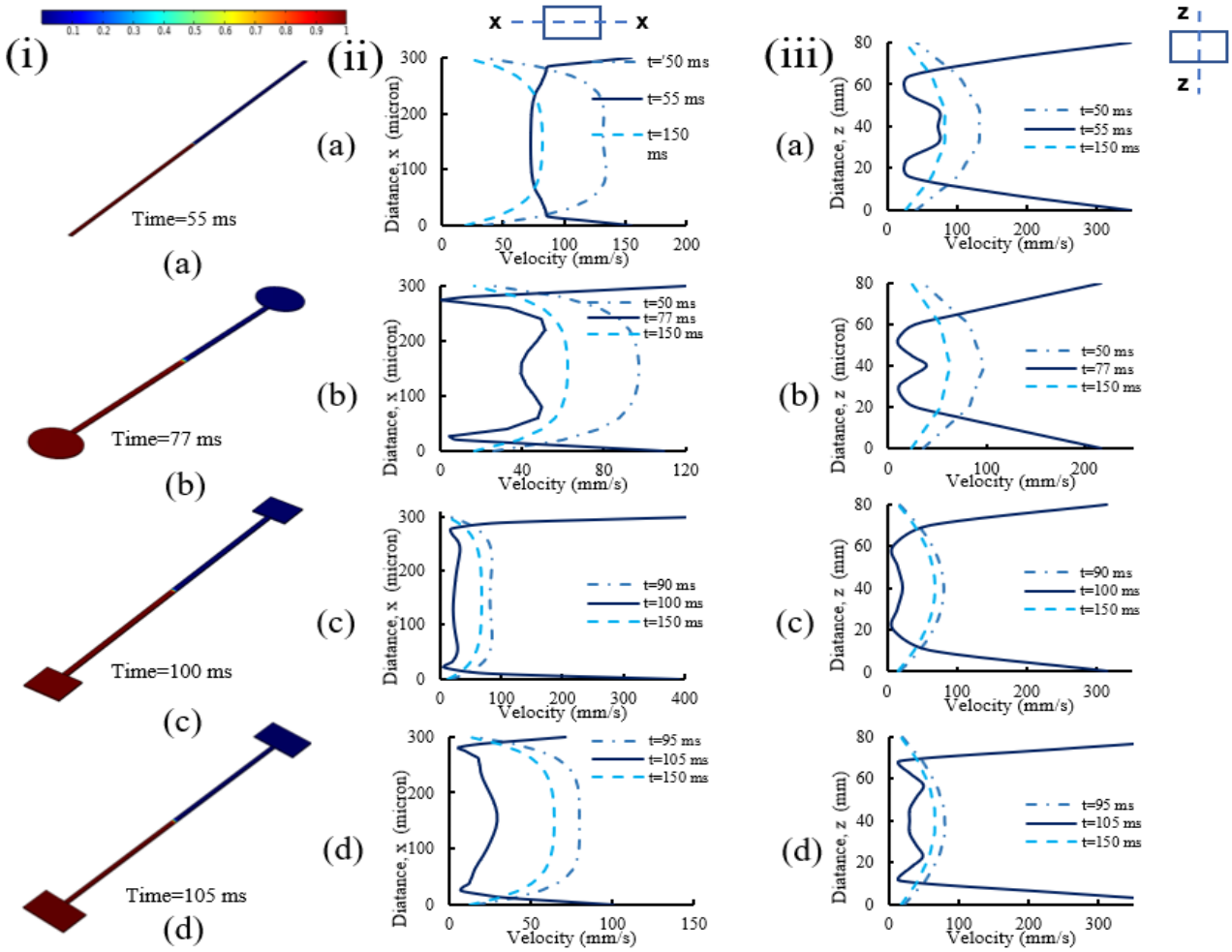

Figure 5: (i) level set contour for (a) extended channel, (b) circular reservoir, (c) square reservoir, (d) rectangular reservoir, (ii) velocity profile in x-axis for (a) extended channel, (b) circular reservoir, (c) square reservoir, (d) rectangular reservoir, (iii) velocity profile in z-axis for (a) extended channel, (b) circular reservoir, (c) square reservoir, (d) rectangular reservoir

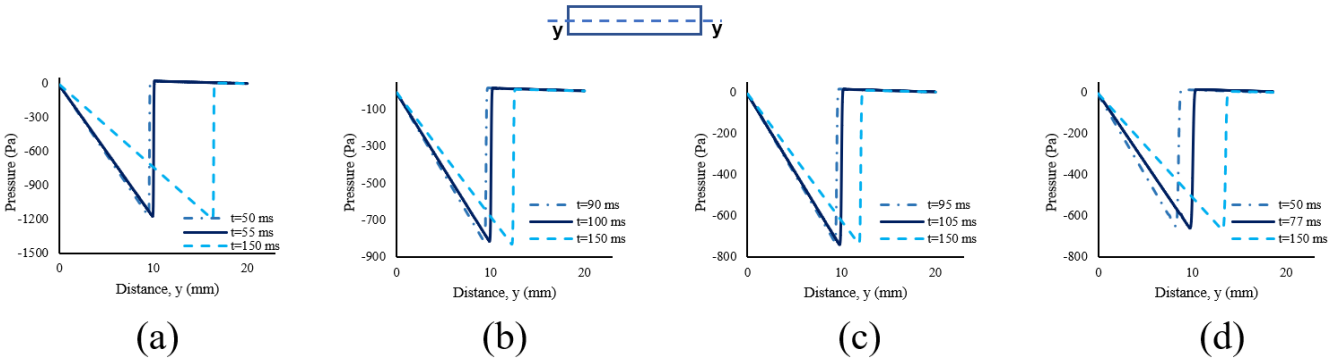

Figure 6: pressure distribution in (A): extended channel, (B): circular reservoir, (C): square reservoir, (D): rectangular reservoir

circular design is estimated more than the two other designs. This means a circular reservoir provides less resistance, decreases flow pressure difference along the microchannel, and increases the flow velocity in the circular design.

H. Conclusion

The effect of reservoir geometry on capillary flow in the microchannel was examined numerically using a microfluidics system with three different reservoir geometries: circular, square, and rectangular design. The laminar two-phase capillary flow (water-air) was simulated using the level-set method inside the 3D microchannel. The Finite Element Method has been used.

The computational velocity distribution along the width and height of the microchannel creates the meniscus shape at the interface and shows high value near walls due to capillary force and surface tension effects at the point of interface. For instance, the velocity along the width of the channel in the circular reservoir increases 2.7 times from the middle of the channel to the walls. Furthermore, simulation results reveal that the geometry of the reservoir affects the capillary flow in the microchannel. Microfluidics design with a circular reservoir has a minimum filling time and rectangular reservoir maximum flow velocity. For example, the time flow needs flow to reach the end of the channel increases in the square and rectangular designs by 6.8% and 13.1% compared to circular design. Also, at the time of $100ms$, the interface position in square and circular designs are 2.7% and 16.2% more than rectangular designs, along the channel, respectively. Therefore, the above analysis indicates the controlling role of the reservoir geometry to change the capillary flow velocity inside a microchannel. Moreover, pressure distribution along the length of the channel shows a suction pressure at the interface point, which causes a jump in the pressure along the channel and indicates the effect of capillary pressure.

REFERENCES

[1] Beebe, D.J., G.A. Mensing, and G.M. Walker, Physics and applications of microfluidics in biology. Annual review of biomedical engineering, 2002. **4**(1): p. 261-286.

[2] Breslauer, D.N., P.J. Lee, and L.P. Lee, Microfluidics-based systems biology. Molecular Biosystems, 2006. **2**(2): p. 97-112.

[3] Chen, J., D. Chen, Y. Xie, T. Yuan, and X. Chen, Progress of microfluidics for biology and medicine. Nano-Micro Letters, 2013. **5**(1): p. 66-80.

[4] Holmes, D. and S. Gawad, The application of microfluidics in biology. Microengineering in biotechnology, 2010: p. 55-80.

[5] Ren, K., Y. Chen, and H. Wu, New materials for microfluidics in biology. Current opinion in biotechnology, 2014. **25**: p. 78-85.

[6] Sackmann, E.K., A.L. Fulton, and D.J. Beebe, The present and future role of microfluidics in biomedical research. Nature, 2014. **507**(7491): p. 181-189.

[7] Sia, S.K. and G.M. Whitesides, Microfluidic devices fabricated in poly (dimethylsiloxane) for biological studies. Electrophoresis, 2003. **24**(21): p. 3563-3576.

[8] Berkenbrock, J.A., R. Grecco-Machado, and S. Achenbach, Microfluidic devices for the detection of viruses: aspects of emergency fabrication during the COVID-19 pandemic and other outbreaks. Proceedings of the Royal Society A, 2020. **476**(2243): p. 20200398.

[9] Dong, X., L. Liu, Y. Tu, J. Zhang, G. Miao, L. Zhang, S. Ge, N. Xia, D. Yu, and X. Qiu, Rapid PCR powered by microfluidics: A quick review under the background of COVID-19 pandemic. TrAC Trends in Analytical Chemistry, 2021. **143**: p. 116377.

[10] Haghayegh, F., Design and development of a microfluidic integrated electrochemical nanobiosensor for detection of SARS-CoV-2 Nucleocapsid protein biomarker. 2021, Schulich School of Engineering.

[11] Liu, D., H. Shen, Y. Zhang, D. Shen, M. Zhu, Y. Song, Z. Zhu, and C. Yang, A microfluidic-integrated lateral flow recombinase polymerase amplification (MI-IF-RPA) assay for rapid COVID-19 detection. Lab on a Chip, 2021. **21**(10): p. 2019-2026.

[12] Ichikawa, N., K. Hosokawa, and R. Maeda, Interface motion of capillary-driven flow in rectangular microchannel. Journal of colloid and interface science, 2004. **280**(1): p. 155-164.

[13] Guo, R., T. Fu, C. Zhu, and Y. Ma, Pressure drop model of gas-liquid flow with mass transfer in tree-typed microchannels. Chemical Engineering Journal, 2020. **397**: p. 125340.

[14] Ma, B., Analysis of capillary flow in a parallel microchannel-based wick structure with circular and noncircular geometries. Langmuir, 2020. **36**(45): p. 13485-13497.

[15] Mikaelian, D. and B. Jones, Modeling of capillary-driven microfluidic networks using electric circuit analogy. SN Applied Sciences, 2020. **2**(3): p. 1-19.

[16] Olanrewaju, A., M. Beaugrand, M. Yafia, and D. Juncker, Capillary microfluidics in microchannels: from microfluidic networks to capillaric circuits. Lab on a Chip, 2018. **18**(16): p. 2323-2347.

[17] Safavieh, R. and D. Juncker, Capillarics: pre-programmed, self-powered microfluidic circuits built from capillary elements. Lab on a Chip, 2013. **13**(21): p. 4180-4189.

[18] Taher, A., B. Jones, P. Fiorini, and L. Lagae, Analytical, numerical and experimental study on capillary flow in a microchannel traversing a backward facing step. International Journal of Multiphase Flow, 2018. **107**: p. 221-229.

[19] Zhu, Y. and K. Petkovic-Duran, Capillary flow in microchannels. Microfluidics and Nanofluidics, 2010. **8**(2): p. 275-282.